Eurographics Workshop on Visual Computing for Biology and Medicine (2014)
I. Viola, K. Bühler, and T. Ropinski (Editors)

Misalignment Correction in Open Cone-Beam CT

A. Wieckowski[1], F. Stopp[2], M. Käseberg[1] and E. Keeve[1,2]

[1]Fraunhofer Institute for Production Systems and Design Technology IPK, Medical Technology, Berlin, Germany
[2]Charité - Universitätsmedizin Berlin, Dept. of Navigation and Robotics, Berlin, Germany

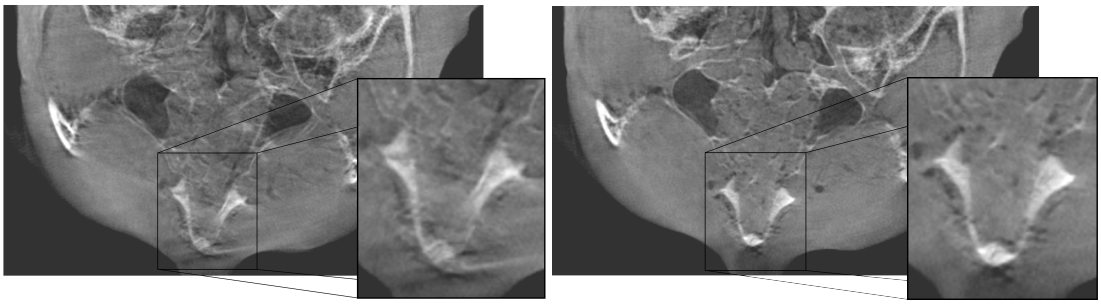

Figure 1: *Axial slices from volumes reconstructed with misaligned and corrected geometry.*

Abstract

Cone-beam computed tomography (CBCT) is an established standard for both, medical and industrial volumetric imaging. To compute a 3D volume, multiple 2D x-ray projection images of an object of interest are acquired from different directions. Using the geometric information about the acquisition geometry of each image, the volume is reconstructed. Incorrect geometric information (misalignments) leads to blurring and other artifacts in the resulting reconstruction.

The exact acquisition geometry is commonly calculated by the analysis of a scan of a dedicated calibration body (off-line calibration). Such approach requires high repeat accuracy of the scanner mechanics and cannot account for non-systematic deviations. Current methods allowing for misalignment correction without a dedicated phantom, e.g. by iteratively adapting the geometry to minimize the arising artifacts, were developed to work with planar trajectories. It poses a problem for open CBCT systems driving complex trajectories.

Therefore, we propose an enhanced method allowing for misalignment correction for general trajectories. We developed a new quality function and a flexible modeling for misalignments. We successfully applied our method to real datasets acquired along planar and non-planar trajectories. The correction with our approach substantially increases the resulting volume quality.

Categories and Subject Descriptors (according to ACM CCS): I.4.3 [Image processing and computer vision]: Enhancement—Geometric correction

1. Introduction

Volumetric imaging is a very important non-invasive diagnostic tool in modern medicine. One of the most commonly used modalities for 3D image acquisition is computed tomography (CT). In cone-beam computed tomography (CBCT), a three-dimensional (3D) representation of an object of interest is obtained by reconstructing it from a set of multiple two-dimensional (2D) x-ray projections acquired at different poses.

The x-ray source and detector are usually rigidly mounted on a frame rotating around the patient. Usual diagnostic scanners employ a closed O-like frame (gantry). The patient has to be placed inside it, so that multiple projection images can be acquired around a circular trajectory by rotating the

DOI: 10.2312/vcbm.20141195

frame around the patient. In intra-operative settings, systems with a C-like gantry (C-arm) are more common. Such systems can be placed around the stationary patient. Fraunhofer IPK, Charité Universitätsmedizin Berlin and Ziehm Imaging GmbH are cooperatively developing a scanner with open patient access – open x-ray scanner for image-guided therapy ORBIT (fig. 2) [SWK*13]. The rigid arrangement of the scanner and detector is dissolved – both are driven by independent robotic mechanism – allowing for driving of new trajectories (fig. 2). Even spontaneous geometry changes in the operating room are thinkable to enhance the quality of a specific region, omit metal implants or to ensure that no collision with other operating equipment is possible.

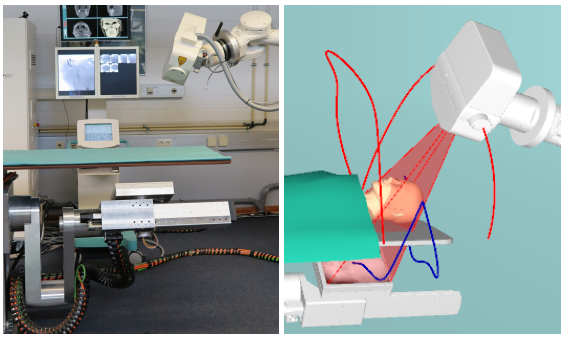

(a) *ORBIT prototype* **(b)** *Exemplary trajectory*

Figure 2: *An open CBCT prototype ORBIT and an exemplary non-planar trajectory.*

The exact knowledge of the pose of the detector and the position of the source for each projection image is required for high-quality reconstructions. If this information is incorrect, artifacts arise in the reconstruction – such inaccuracies are caused by material deformation or limited system resolution. Usually, a system is configured to repetitively drive the same trajectory. Provided it has high repeat accuracy (the geometric errors are always the same), geometry can be estimated once and used in future scans. For the so called off-line calibration, a specially designed calibration body is scanned. The geometric parameters can be calculated by the analysis of the projection images of that body. This is accomplished by comparing detected features on the 2D image plane with their known 3D location in the calibration phantom. Most of such methods are focused on the calibration of circular trajectories [CMSJ05]. More recent methods allow calibration of general trajectories [MCN09] [SWK*13], a requirement for the application with our open CBCT.

For non-systematic misalignments due to spontaneous trajectory changes, low repeat accuracy, or patient movement, the pre-calibrated geometries become obsolete. The misalignments have to be corrected using only the data of the scan itself – no additional calibration scan is possible (see figure 3). Methods like [PBDM08] and [DME*13] employ the redundancy of data in circular scans to accomplish this task. In [WLB11], the authors propose to iteratively align the images with the reconstructed volume. The alignment is achieved by moving the images to a pose in which an artificial projection bears the most similarity with the image.

If the projection geometry of a CBCT dataset is misaligned, the resulting reconstruction contains artifacts. The methods [KLH*08] and [KSV*11] reverse this relationship. The corrected projection geometry is found by adapting the assumed geometry to minimize the resulting reconstruction artifacts. A prerequisite for this approach is an automated measure quantifying the misalignment artifacts present in the reconstruction. In the mentioned methods, slice entropy and sharpness are used. Both methods are designed only for the correction of simple misalignments in circular trajectories. Further quantities are evaluated in [WKKK12] proving volume entropy the most accurate feature for the use-case discussed in [KLH*08].

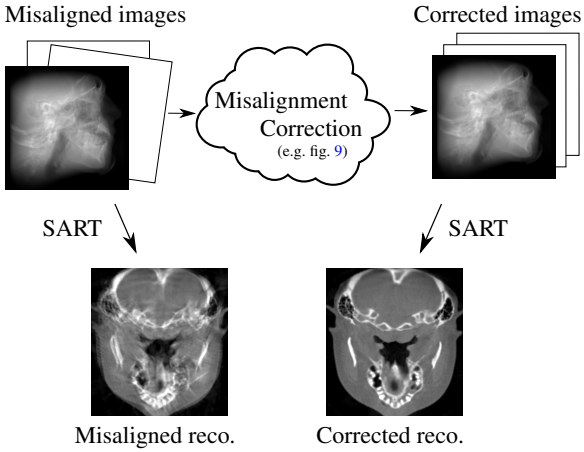

Figure 3: *General flow. The direct reconstruction from the supplied images with misaligned geometry contains artifacts. Misalignment correction reduces the artifacts in the reconstruction by appropriate geometry alignments.*

In this work, we present an extension of the method proposed in [KLH*08]. Most notably, a new robust quality function is presented, which provides very good results for both planar and non-planar trajectories. We also allow for complex modeling of the misalignments.

2. Theory

A CBCT dataset consists of N images I_i ($i = 1 \ldots N$). The nominal projection geometry of each image is described by the 4×4 homogeneous transformation ${}^{B}\mathbf{T}_{D,i}$ describing the pose of the image i in a reference coordinate system B and the 3D position of the x-ray source ${}^{B}\mathbf{s}_i$. The data is misaligned, meaning that the projections were actually acquired with the geometry ${}^{B}\mathbf{T}_{D,i*} \neq {}^{B}\mathbf{T}_{D,i}$ and ${}^{B}\mathbf{s}_{i*} \neq {}^{B}\mathbf{s}_i$.

The reconstruction algorithms inverse the projection relationship. When projecting, all structures (e.g. $\mathbf{r}_1$ and $\mathbf{r}_2$ in fig. 4) along a ray connecting the x-ray source and a detector cell (a pixel in the resulting image – e.g. $\mathbf{p}_1$ and $\mathbf{p}_2$ in fig. 4) contribute to the intensity of the resulting pixel. In the reconstruction, this resulting intensity is distributed in volume by the analysis of all rays passing through the reconstructed voxel. If the geometry is distorted, voxel are reconstructed from rays which did not intersect in the projection – providing inconsistent information. A best fit solution is found for those cases, distributing the intensity of the rays along neighboring voxel. This is analogue to defocused camera lens, which causes the incoming rays from one point to be distributed along a wide patch of detector cells.

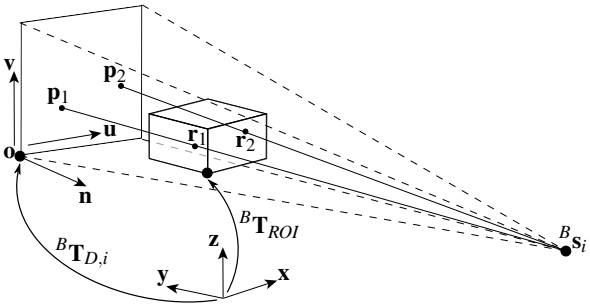

Figure 4: *Projection geometry.*

In figure 5, reconstructions of misaligned CBCT datasets are shown for two different misalignments models. If the misalignments are independent between images, the resulting artifacts look more like general noise. For dependent misalignments (similar for neighboring projection images), the structures are blurred and double edge artifacts arise, depending on the amount of misalignments.

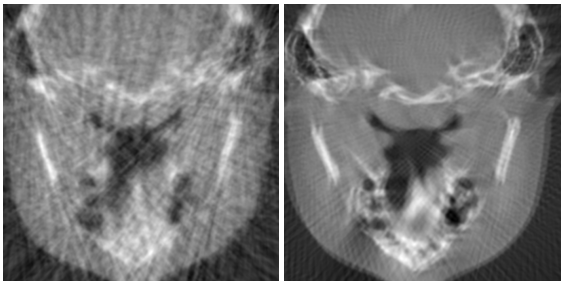

(a) *Independent misalignments* **(b)** *Dependent misalignments*

Figure 5: *Different types of artifacts caused by different misalignments.*

The goal of this method is to find correction terms $\mathbf{T}_{corr}$ and ${}^{B}\mathbf{s}_{i,corr}$ for the nominal geometry resulting in corrected geometry ${}^{B}\mathbf{T}_{D,i'} = {}^{B}\mathbf{T}_{D,i} \cdot \mathbf{T}_{i,corr}$ and ${}^{B}\mathbf{s}_{i'} = {}^{B}\mathbf{s}_{i} + {}^{B}\mathbf{s}_{i,corr}$. Eliminating unnecessary degrees of freedom, the correction matrix $\mathbf{T}_{i,corr}$ can be represented using six parameters (three for the translation and three for the rotation represented in Euler-angles): $\mathbf{T}_{i,corr} = \mathbf{T}_{i,corr}(\alpha_i, \beta_i, \gamma_i, x_i, y_i, z_i)$. The source correction vector is described by the three translational components: ${}^{B}\mathbf{s}_{i,corr} = (x_{s,i}, y_{s,i}, z_{s,i})^T$. Thus, for each projection, nine parameters $\boldsymbol{\xi}_i = (\alpha_i, \beta_i, \gamma_i, x_i, y_i, z_i, x_{s,i}, y_{s,i}, z_{s,i})^T$ need to be found. To correct a whole dataset consisting of N images, a total of $9 \cdot N$ values have to be calculated. The parameter vector $\boldsymbol{\Xi}$ contains all the values ($\boldsymbol{\xi}_i$, $i = 1 \ldots N$) needed to correct a dataset.

3. Method

The method is an enhancement of the method described in [KLH*08]. A prerequisite for quality based misalignment correction is a term for the quantification of the misalignment artifacts – quality function. In the following, we will first describe the method in general. After that, we will discuss the used quality function. Last in our method description, we will discuss the measures allowing for the reduction of calculation time followed by a brief method summary.

3.1. Calculation of misalignments

Given a quality function $Q(\boldsymbol{\Xi})$ measuring the amount of artifacts in the reconstruction applying the corrections $\boldsymbol{\Xi}$, the misalignment correction can be performed by solving the following problem:

$$\boldsymbol{\Xi}_{opt} = \underset{\boldsymbol{\Xi}}{\operatorname{argmin}} Q(\boldsymbol{\Xi}) \tag{1}$$

This approach was derived by assuming that the correct geometry always provides the reconstruction of the best quality or the least artifacts. The problem is solved using numerical optimization.

3.2. Quality Function

A quality function or measure calculates a single real value from a slice reconstruction or a set of reconstructions. Lower values indicate better quality. This behavior is chosen to comply with the conventions of numerical optimization, as the algorithms are usually build to minimize the objective. If a measure is to be maximized, its negative is supplied to the optimization.

Due to calculation cost, Feldkamp-Davis-Kress [FDK84] (FDK) reconstruction is used. Iterative reconstruction methods, although providing better results for non-planar trajectories, do not support single slice reconstruction and take much longer to produce a result. No trajectory dependent adaptations of the FDK reconstruction are implemented. In fact, common Hamming filter along the u-axis is used independent of the trajectory. This causes reconstruction artifacts for non-planar trajectories not caused by misalignment, but rather by non-exact reconstruction. It poses a challenge

for the quality function to distinguish between misalignment and reconstruction artifacts – a problem discussed further on.

First part of our quality function is slice entropy (N_b being the number of histogram bins):

$$H(I) = \sum_{i=1}^{N_b} p_i \cdot \log p_i \tag{2}$$

Although found most accurate in [WKKK12], it proved insufficient in our use-case with more complex misalignments and non-planar trajectories.

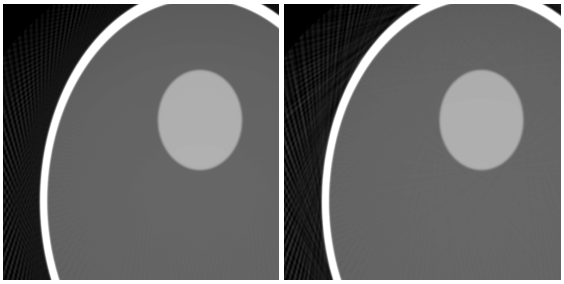

(a) *Initial* **(b)** *Corrected entropy*

Figure 6: *Optimizing a not-misaligned dataset acquired along a circular trajectory (Shepp-Logan phantom [SL74]). The initial reconstruction (a) has very good quality. After entropy optimization, no visible changes can be observed (b).*

We developed a basic test to screen the quality terms for viability. In this test, a simulated dataset (see fig. 7) without misalignments is optimized using a specific quality feature or feature set. The expected result is for the corrections to be negligible. Otherwise, a quality optimum is found for a geometry different than the correct one. For datasets along a planar trajectory, entropy provided the expected correct results (see fig. 6). For a non-planar trajectory (fig. 2b), entropy optimization leads to a wrong minimum. With the found geometry, the initial reconstruction artifacts are blurred out by the arising misalignment artifacts (see fig. 7). To comply with the defined requirements, other quality measures have to be considered.

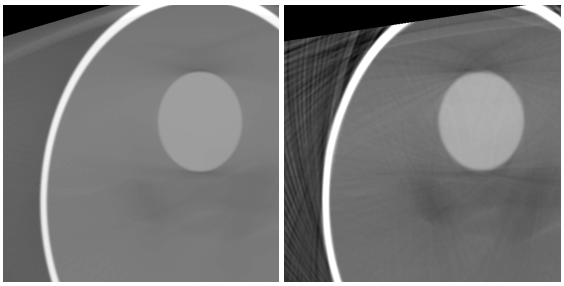

(a) *Initial* **(b)** *Corrected entropy*

Figure 7: *Optimizing a not-misaligned dataset acquired along a non-planar trajectory (Shepp-Logan phantom [SL74]). The reconstruction artifacts in the initial reconstruction (a) increase the entropy more than misalignment artifacts. The optimization (b) introduces misalignment artifacts to overshadow the reconstruction inaccuracies.*

In the field of image reconstruction, total variation (TV) (3) minimization is currently a popular method for quality enhancements [SP08]:

$$tv[I] = \sum_{(x,y)\in P} \|\nabla I(x,y)\| \tag{3}$$

P is the set of all pixels in the image or voxels in the slice reconstruction. This feature (3) is somehow similar to the expression for sharpness as defined in [KSV*11], where it was used to correct simple blurring.

In our use case, with a variety of different artifacts, simple TV did not prove to be a reliable quality feature. Similar conclusions were found in [WKKK12]. In good quality reconstructions of actual structures, edges are usually thin and clear, the regions between them being homogeneous. If geometry misalignments are present, the rays contributing to the edges are not intersecting properly, thus distributing their energy along the homogeneous regions. This causes the reconstructions to contain blurring, double edges or general noise (see figures 5, 10a and 10b). The actual edges become weaker, at the same time the artifacts introduce many false ones, usually of small magnitude. To quantify this behavior, a measure has to penalize introduction of small edges while at the same time ignoring the intensification of actual edges for correct solutions. We propose a simple expression implementing this behavior – saturated total variation:

$$\begin{aligned} \hat{tv}_\mu[I] &= \sum_{(x,y)\in P} S[\|\nabla I(x,y)\|] \\ &= \sum_{(x,y)\in P} \left[2 \cdot \left(1 + e^{-\mu\|\nabla I(x,y)\|}\right)^{-1} - 1\right] \end{aligned} \tag{4}$$

By saturating the gradients before summation, only the gradients in the non-saturated part are penalized. Intensity changes in the saturated area are ignored. The boundary between both areas is governed by μ.

Both the entropy and saturated TV are prone to degenerate solutions if the misalignments become so big, that only noise of small magnitude is contained in the reconstructions. For this reason, we developed regularization for both measures preventing the convergence to those solutions. To regularize the entropy, contrast C, the width of central 90% of the histograms mass normalized to the histogram width, is used. Opposite to the entropy, the contrast is maximized in the optimization. As the histogram has to be created for entropy calculation, the calculation of this additional value comes at a very low cost. Saturated TV provides wrong results when the misalignments are so big, that the actual gradients fall out of the saturated area. To prevent such behavior as being

interpreted as quality improvement, TV (3) maximization is used for regularization.

To contain the optimization within some closed boundaries, a penalty R is added to the optimization objective depending on the magnitude of the corrections. A boundary expression is required because the used numerical optimization algorithm does not provide an integrated boundary setting mechanism. To not bias the correct solutions, the penalty is clipped to zero within the search boundary.

The resulting quality function consist of five terms - entropy and saturated total variation (and the appropriate regularizations) and a penalty term. In the following, the used quality measure is stated in a simplified formulation:

$$Q(I) = H(I) - C(I) + \frac{a \cdot \hat{tv}_{\mu}(I) - b \cdot tv(I)}{|P|} + R \quad (5)$$

Saturated total variation and its regularization are both normalized by the number of voxel used in the calculation of those features. Parameters a and b regulate the scaling of different expressions.

3.3. Method optimization

The reconstruction makes the calculation of $Q(\Xi)$ slow. Modern CBCT system acquire between 100 and 1000 projection images in each scan. This results in more than 1000 and up to 10000 parameters to be estimated for the correction.

In [KLH*08] and [KSV*11], the Downhill-Simplex [NM65] algorithm was used to perform the optimization (1). Due to the ill-posed nature of the problem and the high number of evaluations needed by the optimization algorithm combined with high number of variables and high calculation cost, the problem in its bare formulation is inapplicable for the clinical application. The Downhill-Simplex algorithm provides bad solutions for ill-posed problems [HAR10] and would take too long to calculate them. In the following, measures are discussed to make the method practically applicable.

3.3.1. Dimensionality reduction

In the formulation (1), each possible misalignment is considered independent of the others. In actual CBCT systems, the misalignments are very rarely independent (see figure 5). This assumption is supported by the accuracy measurements of our prototype ORBIT. In C-arm systems, the system deformation is dependent on the angular position of the C-frame. Those dependencies can be used for dimensionality reduction. Similar approach is adapted in [KLH*08], where a corrected circular trajectory is extrapolated from a subset of projections, which are used for optimization. Different than in [KLH*08], in our approach, the optimization does not find a new predefined trajectory (e.g. circular), but rather finds the deviations from the initial trajectory for each single projection image.

To exploit the dependencies, the misalignments are described by a Fourier-Series of order N_f:

$$\zeta_i = \omega_{\zeta,1} + \sum_{j=0}^{N_f} \left[\omega_{\zeta,2j} \cos \frac{2\pi ji}{N} + \omega_{\zeta,2j+1} \sin \frac{2\pi ji}{N} \right] \quad (6)$$

In this equation, ζ can describe any of the nine misalignment dimensions, e.g. $\zeta = x_s$ or $\zeta = \gamma$. The parameters $\omega_{\zeta,i}$ describe the Fourier-Series expanding the dimension ζ. The vector $\mathbf{\Omega}$ describes all of those parameters for all nine dimensions $\zeta \in \{\alpha, \beta, \gamma, x, y, z, x_s, y_s, z_s\}$. Different coding models are thinkable, e.g. polynomial expansion. The Fourier-Series model has proven most advantageous. Using this model, each misalignment dimension can be described with $2 \cdot N_f + 1$ rather than N parameters (usually $N_f = 5 \ldots 10$).

Thus, the problem becomes:

$$\mathbf{\Omega}_{opt} = \underset{\mathbf{\Omega}}{\operatorname{argmin}} Q_f(\mathbf{\Omega}) \quad (7)$$

In (7), $Q_f(\mathbf{\Omega}) = Q(\Xi(\mathbf{\Omega}))$ describes the quality function analogue to the one in (1), but applying the transformation (6). The resulting parameter set $\mathbf{\Omega}_{opt}$ has to be transformed into Ξ by the means of the transformation (6).

Further dimensionality reduction can be achieved by setting $\zeta_i = 0 \forall i = 1 \ldots N$ meaning no correction for a specified dimension, e.g. x-ray source position. Such a simplification can be used if the accuracy – or repeat accuracy provided a pre-calibration is available – of a system component is known and sufficient. If the misalignments are independent, a direct model can be applied: $\zeta_i = \omega_{\zeta_i}$.

The resulting problems, although substantially simplified, are still complex, highly-dimensional and ill-defined – not well suited to be solved using the Downhill-Simplex algorithm. In [HAR10], covariance matrix adaptation evolution strategy (CMA-ES) [Han06] was identified to perform best for this kind of problems. We successfully incorporated CMA-ES as the optimization routine into our misalignment correction framework. Despite its randomized nature it constantly provides reliable results.

3.3.2. Reduction of calculation cost

In [KLH*08], [KSV*11] as well as this method, FDK reconstruction is used. Although possibly very fast (using a GPGPU implementation), it still remains the bottleneck for the calculation of the cost function. The reconstruction cost is dependent on the volume size and the number and resolution of the projection images. To reduce this cost, rather than reconstructing the whole volume, only single slices are selected, representative of the whole volume – containing the artifacts that would arise at different locations and angles.

In the mentioned methods, central axial slice and possibly

two parallel slices offset along the axis of rotation are used. This is motivated by the fact, that this slice is most accurately reconstructed when working with circular trajectories. For arbitrary non-planar trajectories, no such slice can be generally selected. A set of slices arranged by rotating a base slice around its axes is reconstructed (see fig. 8). Usually 9 or 13 slices are reconstructed, reducing the reconstruction cost by about the factor of 20 for 256^3 volumes.

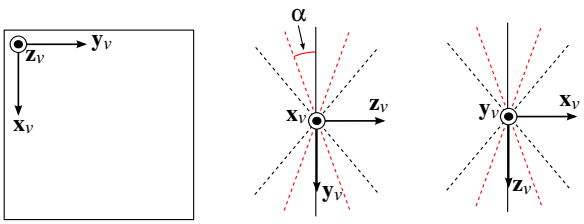

Figure 8: *The arrangement of the slices reconstructed for quality assessment of the volume. A base slice spanned by the vectors $\mathbf{x}_v$ and $\mathbf{y}_v$ is rotated at its middle by the both spanning axes.*

The usage of the reconstruction use-case differs substantially from the usual case. Rather than reconstructing big volumes from different datasets, small slices are reconstructed from the same image data at a high pace – only the pose information for the slice (allowing for reconstruction of different slices) and the images change between reconstructions (applying the corrections). The GPGPU FDK implementation [KMK13] was adapted to allow for the modification of geometry information between reconstruction without additional image data upload.

3.3.3. Correction process

Figure 9 shows the flow diagram of the misalignment calculation process as described previously. The algorithm is initialized assuming that the nominal pose information is correct. In each optimization step, the correction terms are adapted and the resulting slice reconstruction quality is evaluated. The optimization algorithm learns the topology of the underlaying problem and tries to adapt the corrections in the directions of the optimum – e.g. for CMA-ES, the topology information is stored in a covariance matrix. If no further quality improvement can be found, the process is completed. The resulting optimal geometry is used to calculate the corrected reconstruction with the SART algorithm [AK84] (simultaneous algebraic reconstruction technique).

4. Evaluation

The quality function should indicate the amount of artifacts in the reconstruction – it should rise with increasing misalignments causing more artifacts. In [WKKK12], an evaluation method for different quality functions is proposed. A set of reconstructions is carefully prepared so that each corresponds to a different misalignments level. In [WKKK12], the misalignment level is measured using an effective universal measure – back projection mismatch (BPM) [WKV*11]. The quality of each of the reconstructions is than assessed using a quality feature. The accuracy of the tested feature is quantified as the agreement between the ground truth (BPM) and the assessment of that feature.

We follow a similar approach. We prepared misaligned reconstructions with increasing misalignment levels (see figures 10b and 10a) and calculated the value of our quality function for each of the reconstructions. Rather than reducing the arising curves to a single value (e.g. accuracy), we analyze those curves and discuss the arising optimization manifold.

In figure 10, the quality evaluation of the prepared reconstructions with different quality measures is shown. Measurement of the quality using our new function and the expressions composing it (entropy and saturated total variation – with and without regularization) are plotted.

For a quality function, the desired outcome is to always assign a better score to a reconstruction with a lower misalignment level. If this property is not assured, local minimums arise. Although the optimization algorithm used in the implementation can in some extent overcome such obstacles, they are still undesirable.

In the first plot showing the scoring of entropy as qual-

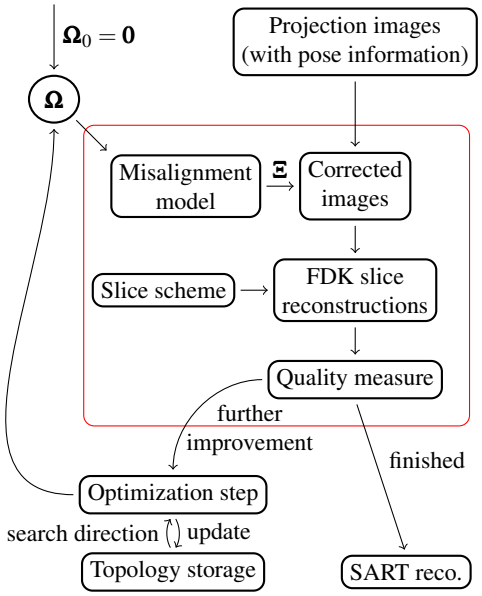

Figure 9: *Flow diagram of the misalignment correction (see fig. 3). The red rectangle emphasizes the steps needed for quality measure calculation for specified misalignments $\mathbf{\Omega}$.*

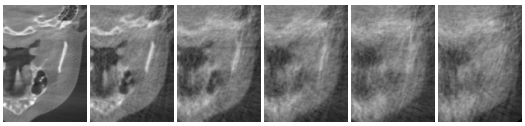

(a) *An exemplary increasingly misaligned dataset (---).*

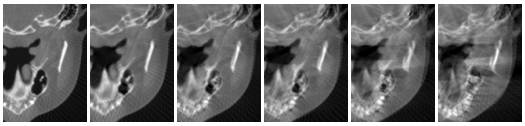

(b) *An exemplary dataset with dependent misalignments (---).*

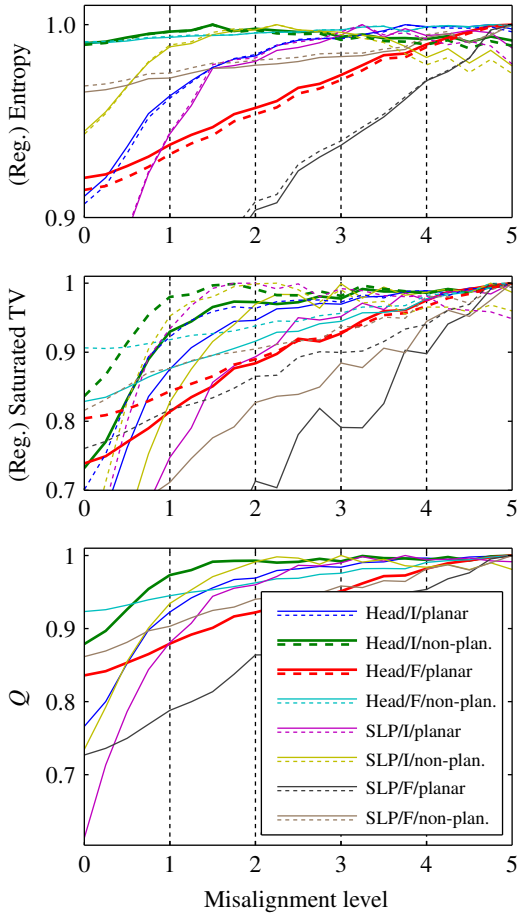

(c) *Misalignment quantification Q and the features composing (5) for increasingly misaligned datasets (normalized to maximum 1). Different curves denote the evaluation of different datasets with head or Shepp-Logan (SLP) phantom, independent (I) or Fourier-series dependent (F) modeled misalignments and non-planar or planar trajectory. Dashed lines indicate not regularized features. Two of the datasets are emphasized and pictured in a and b.*

Figure 10: *The misalignment quantification for increasingly misaligned datasets.*

ity feature, it is apparent that wrong assessment is provided for non-planar trajectory. Most notably, for the simulations with the head phantom acquired along a non-planar trajectory, the scores assigned to not misaligned reconstruction are only slightly better than the scores of reconstructions with severe artifacts. At very high misalignment levels, the score drops creating a local minimum, which is not easily escaped – a big enough initial search scope has to be provided. The effects of the regularization are small, but clear – the score dropping for high misalignment levels is counteracted. Entropy provides a very good quality assessment for reconstructions of datasets simulated along a circular trajectory. Those findings are consistent with both [WKKK12] and the conclusions discussed in section 3.2.

Saturated total variation provides much more consistent quality assessment. When regularized with total variation (solid line), a consistent evaluation of the level of artifacts is provided independent of the phantom, trajectory and type of misalignments. Different than with entropy, the regularization effects are very strong in this case. For independent misalignments, a saturation of the quality function can be observed at about misalignment level 2, after which the score indicates no further quality reduction. For the easier Shepp-Logan phantom, the score even gets better. The regularization eliminates this effect. Some minor local minimums are still observable, but the used optimization algorithm can escape such minor obstacles.

The final quality function – a combination of regularized entropy and regularized saturated total variation – combines the advantages of both quality features. The function consistently provides accurate assessment of the amount of misalignment artifacts – independent of trajectory, type of misalignments or the pictured structure. For independent misalignments, the scoring saturates at about the level 3. This behavior is expected – the reconstruction at misalignment level 3 does not really provide more useful information than the one at the level 5.

5. Results

We applied our method to both simulative and real misaligned datasets. In the following, three of the results are presented. We tested the method with real scans of a head phantom. The horizontal lines visible in the sagittal views in figure 12 and 13 are caused by the phantom structure. Empty spaces between the slices assembling the phantom are the cause for those lines.

5.1. Simulation with a head phantom

Result of an exemplary simulation is pictured in fig. 11. A dataset consisting of 200 images along a non-planar trajectory (see fig. 2b) was simulated. The geometry was misaligned using a dependent model at level 2 (compare fig. 10b). Using our simulation environment, projection images

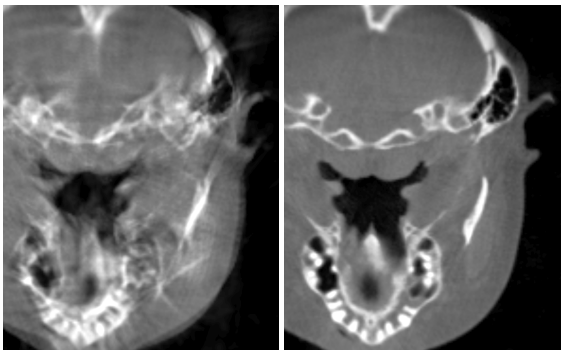

(a) *Misaligned* **(b)** *Corrected*

Figure 11: *Misaligned and corrected SART reconstructions of a head phantom simulated dataset acquired along a non-planar trajectory.*

of a CT-volume were acquired at the misaligned positions. The slice 11a shows a SART reconstruction of that dataset using the nominal geometry. Using the nominal geometry as the initialization, we optimized the volume quality as described previously. Figure 11b shows a slice from the SART reconstruction with the corrected geometry. All of the visible artifacts like blurring and double edges are eliminated. In the resulting reconstruction, all anatomical structures can be clearly recognized. Fourier-series ($N_f = 5$) model for corrections was used as the misalignments are not independent (compare fig. 5). The optimization took about 5 minutes to complete on an up-to-date multi-core computer.

5.2. Application with a C-arm

We tested our application with a misaligned dataset acquired with a conventional C-arm cone-beam CT. The dataset consists of 441 images acquired along a circular trajectory along 200°. No information about the amount of geometry deviation is available for this dataset, nor could a reference reconstruction be obtained. We applied our correction method. Fourier-series model ($N_f = 5$) for corrections was used. Two slices of the misaligned and corrected reconstructions are shown in figure 12. The quality gets substantially improved. Double-edge artifacts and blurring are mostly removed, revealing much finer details in the resulting volume. The optimization took about 5 minutes to complete.

5.3. Application with an open cone-beam CT

To test the method in an actual application, we acquired 512 images of the Alderson RANDO head phantom with our prototype of an open CBCT (see fig. 2a) on a not off-line calibrated non-planar trajectory (see fig. 2b). The axial slices and teeth cross-sections of the uncorrected, corrected and reference reconstructions are shown in figure 13. The reference volume was acquired by an additional off-line cali-

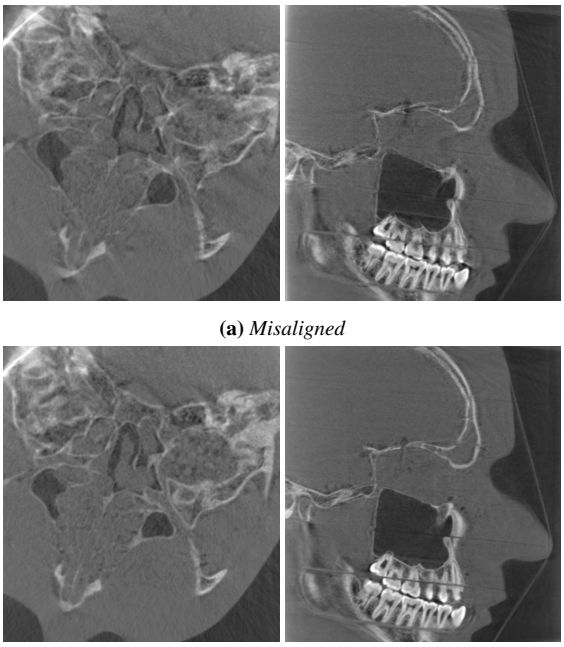

(a) *Misaligned*

(b) *Corrected*

Figure 12: *Misaligned and corrected SART reconstructions of the Alderson RANDO phantom acquired with a conventional C-arm system along a planar trajectory. The central axial slice and the teeth cross-section is shown.*

bration of the driven trajectory using the method described in [SWK*13]. Most of the initial artifacts were successfully corrected, substantially increasing the volume quality. The pictured structures become much clearer after correction, allowing for inspection of much finer details. Fourier-series ($N_f = 5$) model was used for corrections. The optimization took about 10 minutes to complete.

The provided quality is not yet comparable to the quality achievable with off-line calibration. Compared to the reference, the corrected volume still contains some artifacts. Mostly mild blurring is noticeable at the edges of bony structures and air blisters. The reference reconstruction also allows to qualitatively assess the amount of misalignments artifacts present in the dataset.

6. Discussion

The method is still under active development. Currently under investigation is the issue, that the algorithm optimizes the volume quality by geometry changes without any reference to an external coordinate system. Any registration between the volume coordinate system and an external reference system is lost. A rigid transformation of the whole geometry within the optimization bounds would not influence the reconstruction quality – only move the contents of the volume.

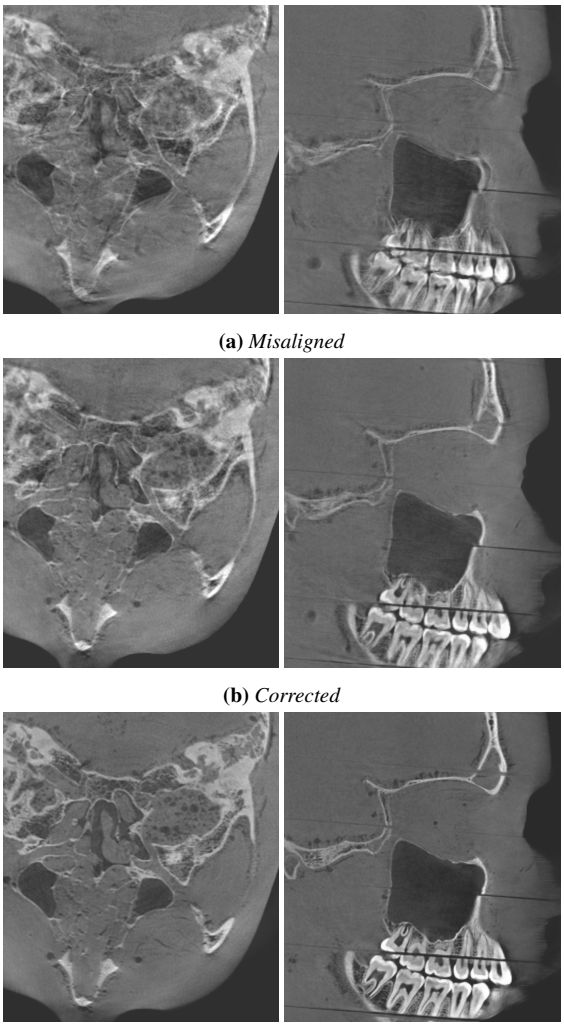

(a) *Misaligned*

(b) *Corrected*

(c) *Reference*

Figure 13: *Misaligned, corrected and reference SART reconstructions of the Alderson RANDO phantom acquired along an non-planar trajectory (see fig. 2b). The central axial slice and a sagittal slice are shown. The misalignment correction was initialized with the nominal geometry. The reference reconstruction was obtained by an off-line calibration of the driven trajectory.*

For this reason the method is so far incompatible with navigated applications.

Further, no automated parameter calculation is yet provided. The exact parametrization depends on the contrast of the initial reconstruction and the level of misalignments. We prepared some presets for the identified typical cases, but a fully automated estimation is not currently available.

There are many not yet evaluation parameters which could possibly influence the quality of the resulting reconstruction. Exemplary, increasing the resolution of the slices used in optimization might reveal finer artifacts.

The mentioned optimization times of 5 to 10 minutes needed for the correction were recorded on an up-to-date developer workstation with a single GPU. In the CMA-ES algorithm, multiple cost function evaluation are called independently every iteration. With multiple reconstruction units (GPUs), the workload could be split fairly providing almost linear scaling. Such multi-GPU workstations are not uncommon in modern operating rooms, due to the need for fast reconstruction. Also, in the current implementation, the method calculates the quality measures on the CPU after downloading the reconstructed slice. Moving those calculations to the GPU would further shrink the amount of data exchange increasing the reconstruction rate.

7. Conclusions

We propose an enhanced method for misalignment correction in open cone-beam CT. It can be applied to both circular and arbitrary trajectories. Flexible modeling allows for trade-offs between performance and accuracy. A new robust function for the assessment of misalignment artifacts is presented.

Our method performs very well both in simulation and application. We applied our approach to the scans of a not off-line calibrated trajectories with very good results. The resulting volume quality, although very good, is not yet as good as can be provided with the golden standard – off-line calibration. Still, the provided quality is by far superior to reconstruction without corrections. The method allows for spontaneous trajectory adaptations in the operating room. This is most advantageous for open cone-beam CT (e.g. ORBIT), which can drive a variety of different trajectories.

Acknowledgment

This work is funded by the German Federal Ministry of Education and Research (BMBF), research grant 01EZ1115A.

References

[AK84] ANDERSEN A. H., KAK A. C.: Simultaneous algebraic reconstruction technique (SART): a superior implementation of the ART algorithm. *Ultrasonic imaging 94*, 1 (1984), 81–94. doi:10.1016/0161-7346(84)90008-7. 6

[CMSJ05] CHO Y., MOSELEY D. J., SIEWERDSEN J. H., JAFFRAY D. A.: Accurate technique for complete geometric calibration of cone-beam computed tomography systems. *Medical Physics 32*, 4 (2005), 968–983. URL: http://scitation.aip.org/content/aapm/journal/medphys/32/4/10.1118/1.1869652, doi:10.1118/1.1869652. 2

[DME*13] DEBBELER C., MAASS N., ELTER M., DENNERLEIN F., BUZUG T. M.: A New CT Rawdata Redundancy Measure applied to Automated Misalignment Correction. In *12th International Meeting on Fully Three-Dimensional Image Recon-*

struction in Radiology and Nuclear Medicine (2013), pp. 264–267. 2

[FDK84] FELDKAMP L., DAVIS L., KRESS J.: Practical cone-beam algorithm. *J. Opt. Soc. Am. A 1*, 6 (Jun 1984), 612–619. 3

[Han06] HANSEN N.: The CMA Evolution Strategy: A Comparing Review. In *Towards a New Evolutionary Computation*, Lozano J. A., Larrañaga P., Inza I. n., Bengoetxea E., (Eds.), vol. 192 of *Studies in Fuzziness and Soft Computing*. Springer Berlin Heidelberg, 2006, pp. 75–102. URL: http://link.springer.com/chapter/10.1007/3-540-32494-1_4, doi:10.1007/3-540-32494-1_4. 5

[HAR10] HANSEN N., AUGER A., ROS R.: Comparing results of 31 algorithms from the black-box optimization benchmarking BBOB-2009. In *Proceedings of the 12th Annual Conference Companion on Genetic and Evolutionary Computation* (New York, NY, USA, 2010), GECCO '10, ACM, pp. 1689–1696. URL: http://dl.acm.org/citation.cfm?id=1830790, doi:10.1145/1830761.1830790. 5

[KLH*08] KYRIAKOU Y., LAPP R. M., HILLEBRAND L., ERTEL D., KALENDER W. A.: Simultaneous misalignment correction for approximate circular cone-beam computed tomography. *Physics in Medicine and Biology 53*, 22 (Nov. 2008), 6267–6289. URL: http://iopscience.iop.org/0031-9155/53/22/001/, doi:10.1088/0031-9155/53/22/001. 2, 3, 5

[KMK13] KÄSEBERG M., MELNIK S., KEEVE E.: OpenCL Accelerated Multi-GPU Cone-Beam Reconstruction. In *12th International Meeting on Fully Three-Dimensional Image Reconstruction in Radiology and Nuclear Medicine* (2013), pp. 447–450. 6

[KSV*11] KINGSTON A., SAKELLARIOU A., VARSLOT T., MYERS G., SHEPPARD A.: Reliable automatic alignment of tomographic projection data by passive auto-focus. *Medical physics 38*, 9 (Sept. 2011), 4934–45. URL: http://www.ncbi.nlm.nih.gov/pubmed/21978038, doi:10.1118/1.3609096. 2, 4, 5

[MCN09] MENNESSIER C., CLACKDOYLE R., NOO F.: Direct determination of geometric alignment parameters for cone-beam scanners. *Physics in Medicine and Biology 54*, 6 (2009), 1633–1660. doi:10.1088/0031-9155/54/6/016. 2

[NM65] NELDER J. A., MEAD R.: A simplex method for function minimization. *The Computer Journal 7*, 4 (1965), 308–313. URL: http://comjnl.oxfordjournals.org/content/7/4/308.short, doi:10.1093/comjnl/7.4.308. 5

[PBDM08] PANETTA D., BELCARI N., DEL GUERRA A., MOEHRS S.: An optimization-based method for geometrical calibration in cone-beam CT without dedicated phantoms. *Physics in Medicine and Biology 53*, 14 (July 2008), 3841–61. URL: http://stacks.iop.org/0031-9155/53/i=14/a=009, doi:10.1088/0031-9155/53/14/009. 2

[SL74] SHEPP L., LOGAN B.: The fourier reconstruction of a head section. *IEEE Transactions on Nuclear Science 21*, 3 (June 1974), 21–43. doi:10.1109/TNS.1974.6499235. 4

[SP08] SIDKY E. Y., PAN X.: Image reconstruction in circular cone-beam computed tomography by constrained, total-variation minimization. *Physics in Medicine and Biology 53*, 17 (2008), 4777. URL: http://stacks.iop.org/0031-9155/53/i=17/a=021, doi:10.1088/0031-9155/53/17/021. 4

[SWK*13] STOPP F., WIECKOWSKI A. J., KÄSEBERG M., ENGEL S., FEHLHABER F., KEEVE E.: A Geometric Calibration Method for an Open Cone-Beam CT System. In *12th International Meeting on Fully Three-Dimensional Image Reconstruction in Radiology and Nuclear Medicine* (2013), pp. 106–109. 2, 8

[WKKK12] WICKLEIN J., KUNZE H., KALENDER W. A., KYRIAKOU Y.: Image features for misalignment correction in medical flat-detector CT. *Medical Physics 39*, 8 (Aug. 2012), 4918–4931. URL: http://www.ncbi.nlm.nih.gov/pubmed/22894418, doi:10.1118/1.4736532. 2, 4, 6, 7

[WKV*11] WICKLEIN J., KUNZE H., VOGT F., KYRIAKOU Y., KALENDER W. A.: An Object-Independent Measure for Improving Misalignment Correction in C-Arm CT. In *11th International Meeting on Fully Three-Dimensional Image Reconstruction in Radiology and Nuclear Medicine* (2011), pp. 148–151. 6

[WLB11] WEIN W., LADIKOS A., BAUMGARTNER A.: Self-calibration of geometric and radiometric parameters for cone-beam computed tomography. In *11th International Meeting on Fully Three-Dimensional Image Reconstruction in Radiology and Nuclear Medicine* (2011), pp. 327–330. 2